https://doi.org/10.3847/2041-8213/aae077

Fermi-LAT Observations of the 2017 September 10 Solar Flare

Nicola Omodei[1], Melissa Pesce-Rollins[2], Francesco Longo[3,4], Alice Allafort[1], and Säm Krucker[5,6]
[1] W. W. Hansen Experimental Physics Laboratory, Kavli Institute for Particle Astrophysics and Cosmology, Department of Physics and SLAC National Accelerator Laboratory, Stanford University, Stanford, CA 94305, USA; nicola.omodei@stanford.edu
[2] Istituto Nazionale di Fisica Nucleare, Sezione di Pisa, I-56127 Pisa, Italy; melissa.pesce.rollins@pi.infn.it
[3] Istituto Nazionale di Fisica Nucleare, Sezione di Trieste, I-34127 Trieste, Italy; francesco.longo@trieste.infn.it
[4] Dipartimento di Fisica, Università di Trieste, I-34127 Trieste, Italy
[5] Space Science Laboratory, University of California, Berkeley, CA 94720-7450, USA
[6] University of Applied Sciences and Arts Northwestern Switzerland, CH-5210 Windisch, Switzerland
Accepted 2018 September 9

Abstract

The *Fermi*-Large Area Telescope detection of the X8.2 *GOES* class solar flare of 2017 September 10 provides for the first time observations of a long-duration high-energy gamma-ray flare associated with a ground-level enhancement (GLE). The >100 MeV emission from this flare lasted for more than 12 hr covering both the impulsive and extended phases. We present the localization of the gamma-ray emission and find that it is consistent with the active region from which the flare occurred over a period lasting more than 6 hr. The temporal variation of the gamma-ray flux and of the proton index inferred from the gamma-ray data seems to suggest three phases in acceleration of the proton population. Based on timing arguments we interpret the last phase to be tied to the acceleration mechanism powering the powering the production of the GLE particles.

Key words: Sun: flares – Sun: X-rays, gamma rays

1. Introduction

High-energy gamma-ray solar flares provide the unique opportunity to examine pion-decay emission at the Sun. In order for this emission to occur, >300 MeV protons must be accelerated and subsequently interact with the chromosphere. Observations of prolonged pion-decay emission from flares (Forrest et al. 1985; Kanbach et al. 1993; Ryan 2000; Chupp & Ryan 2009) brought forth the idea that solar energetic particles (SEPs) could be linked to these long-duration gamma-ray flares (LDGRFs) through coronal and interplanetary shocks.

Fermi-Large Area Telescope (LAT; Atwood et al. 2009) observations of the Sun have drastically increased the population of LDGRFs, including hour-long emission from flares originating from active regions (ARs) located behind the visible disk of the Sun (Ackermann et al. 2014; Ajello et al. 2014; Ackermann et al. 2017).

These observations, as well as observations of previous flares (Vestrand & Forrest 1993; Cliver et al. 1993), indicate that energetic particles are transported onto the visible disk with an accompanying AR behind the limb. We also note that all of the LDGRFs observed by *Fermi*-LAT are also associated with fast coronal mass ejections (CMEs; Ackermann et al. 2014). In addition to this, SEPs are also thought to be accelerated via shocks, and thus it is natural to search for a link between LDGRFs, SEPs, and CMEs (Share et al. 2017, and also Winter et al. 2018).

In this Letter we present the *Fermi*-LAT observations of the 2017 September 10 solar flare associated with the second GLE of the solar cycle. We present-time-resolved the localization of the >100 MeV emission and spectral evolution including the inferred proton index during the more than 12 hr duration of emission.

2. Observations and Data Analysis

After almost an entire year of a nearly spotless Sun and no flaring activity, the largest flare (*GOES* class X9.3) of the solar cycle erupted from AR 2673 on 2017 September 6. This flare was very bright in gamma-rays and the emission detected by *Fermi*-LAT lasted for almost 15 hr (Longo et al. 2017). Only four days later, on September 10 at 15:35 UT, a *GOES* X8.2 class flare (SOL2017-09-10) erupted from the same AR, which had moved to the edge of the western solar limb (S08W88). This flare led to a gradual SEP event with proton energies measured by the *GOES* spacecraft exceeding 700 MeV/n and a very fast CME erupting over the western limb. The first appearance of the CME by LASCO C2 was at 16:00:07 UT and the initial speed was 3620 km s^{-1}. This flare was also associated with the second GLE (#72) of this solar cycle. The GLE 72 onset was observed by several neutron monitors at 16:15 UT, but the strongest increase in count rate was observed at 16:30 UT at the Dome C station, installed in the inner Antarctic Plateau, at Concordia station (Mishev et al. 2018).

Extreme ultraviolet (EUV) observations from the *Solar Dynamics Observatory*/Atmospheric Imaging Assembly (*SDO*/AIA) and the Solar Ultraviolet Imager (SUVI) revealed flare loops seen above the limb that form a flare arcade (for EUV images see Li et al. 2018; Seaton & Darnel 2018; Warren et al. 2018; Yan et al. 2018). The arcade was seen face-on for the part of the flare closest to the limb, while the arcade twisted toward the south making it partially seen side-on for the more distant part of the arcade (see Figure 3 in Seaton & Darnel 2018). The absence of *STEREO* B imaging for this flare unfortunately limits our knowledge of details of the flare geometry. However, the available data sets clearly indicate a two-ribbon flare geometry for SOL2017-09-10. The *Reuven Ramaty High Energy Solar Spectroscopic Imager* (*RHESSI*) had good coverage of the impulsive phase with a peak time of the non-thermal >30 keV HXR emission around 15:59 UT. *RHESSI* high-resolution imaging at 2″ angular resolution showed a single non-thermal hard X-ray (HXR) source above 30 keV located about ∼1″ above the solar limb. Below 20 keV, *RHESSI* observed thermal emission from the flare loops (see insert in Figure 3). Compared to the flare

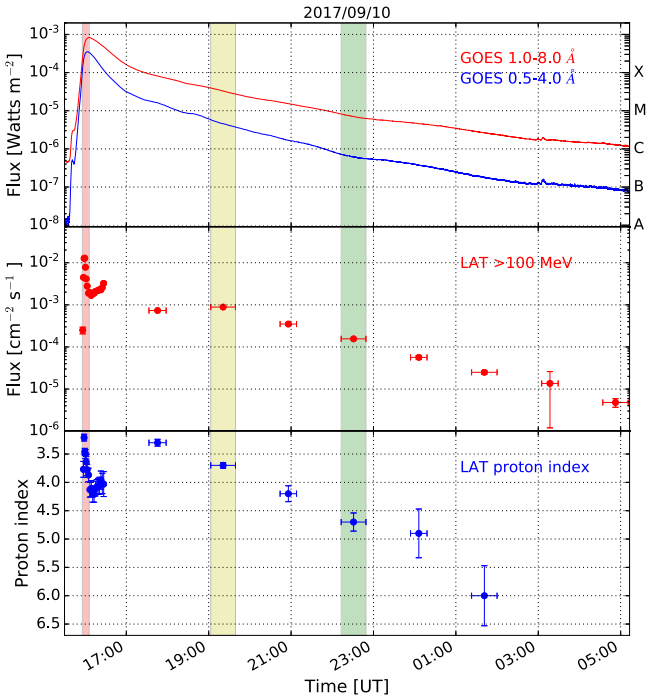

Figure 1. Composite light curve for the 2017 September 10 flare with data from *GOES* X-rays, *Fermi*-LAT >100 MeV flux, and the best proton index inferred from the LAT gamma-ray data. The three color bands represent the time windows over which we performed the localization of the gamma-ray emission, shown in Figure 3.

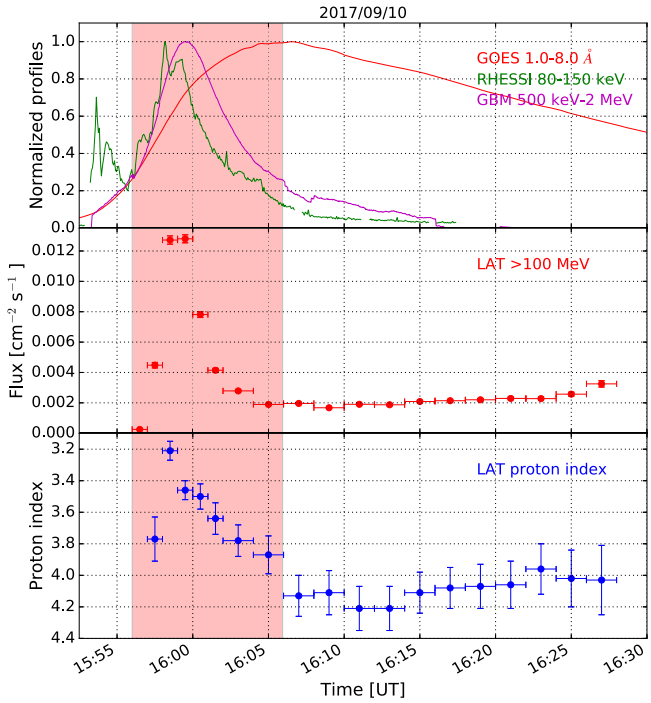

Figure 2. Composite light curve for the impulsive phase of the 2017 September 10 flare with data from *GOES*, *RHESSI*, *Fermi*-GBM, and *Fermi*-LAT. The bottom panel reports the best proton index in each time interval in which the LAT detected the flare. Only GBM-BGO data are shown because NaI suffered from pile-up. The red color band represents the time window over which the localization was performed and is shown in red in Figure 3.

loops, the non-thermal HXR source came from the southern flare ribbon. The corresponding emission from the northern ribbon appeared to be occulted from Earth view. Despite the fact that only one flare footpoint is seen in HXRs, SOL2017-09-10 has one of the highest fluxes at 30 keV (~45 photons cm^{-2} s^{-1} keV^{-1}) compared to statistical studies of large *RHESSI* flares (e.g., Kuhar et al. 2016). The visible HXR footpoint was observed to be co-spatial with the optical signal seen by *SDO*/Helioseismic and Magnetic Imager (HMI) at 617 nm (see insert in Figure 3; for similar events see Krucker et al. 2015). While it remains unclear if the HXR footpoint occurred right above the limb or slightly behind or in front, we firmly conclude that no HXR emission is detected on the visible disk, indicating that no part of the flare ribbons are on disk as seen from Earth view.

The >100 MeV emission detected by the LAT lasted for 12 hr and for that time period the Sun was the brightest gamma-ray source in the sky (see ATel 10721 for further details). The onset time for the LAT was found to be at 15:56 UT, the peak flux occurred at 15:59 UT remaining statistically significant until September 11, 05:11 UT. During the flare, the LAT detected 130 photons with measured energy greater than 1 GeV and reconstructed direction less than 1° from the center of the solar disk.

In Figure 1 we plot the light curves from *GOES* and *Fermi*-LAT for the full 12 hr detection period, while in Figure 2 we plot *GOES*, *RHESSI*, *Fermi*-Gamma-Ray Burst Monitor (GBM), and *Fermi*-LAT intensities for the impulsive phase only. The bottom panel of each figure reports the best proton index in each time interval in which the LAT detected the flare. In Section 2.1 we describe how we obtain the protons index from the gamma-ray emission.

2.1. Spectral Analysis

We performed an unbinned likelihood analysis of the *Fermi*-LAT data with the `gtlike` program distributed with the *Fermi* `ScienceTools`.[7] In order to avoid possible effects from pile-up in the anti-coincidence detector of the LAT during the brightest phase of the flare, from 15:54 to 16:28 UT we selected the Pass 8 Solar flare Transient class (S15)[8] to perform our spectral analysis. This new transient class was developed to be insensitive to the high flux of X-rays often present during bright solar flares. For the remainder of the observation time (from 17:33 to the end of the detection), we used Pass 8 Source class events. For the entire detection time we used selected photons from a 10° circular region centered on the Sun and within 100° from the local zenith (to reduce contamination from the Earth limb).

Following the same approach as Ajello et al. (2014), Pesce-Rollins et al. (2015), and Ackermann et al. (2017), we fit three models to the *Fermi*-LAT gamma-ray spectral data. The first two, a pure power law (PL) and a power law with an exponential cutoff (PLEXP) are phenomenological functions that may describe bremsstrahlung emission from relativistic electrons. The third model uses templates based on a detailed study of the gamma-rays produced from the decay of pions originating from accelerated protons with an isotropic pitch angle distribution in a thick-target model (updated from Murphy et al. 1987). We rely on the likelihood ratio test and the associated test statistic (TS; Mattox et al. 1996) to estimate

[7] We used the version 11-05-03 available from the *Fermi* Science Support Center http://fermi.gsfc.nasa.gov/ssc/.

[8] TRANSIENT015 is available in the extended photon data through the Fermi Science Support Center.

Table 1
Fermi-LAT Spectral Analysis of the Solar flare of 2017 September 10

Time Interval (UT)	TS_{PL}	ΔTS[a]	Photon Index[b]	Cutoff Energy[c] (MeV)	Flux[d] ($\times 10^{-5}$ ph cm^{-2} s^{-1})	Proton Index
15:56:55–15:57:55	116	14	-2.2 ± 0.2	⋯	22 ± 4	⋯
15:57:55–15:58:54	9600	118	-0.8 ± 0.2	211 ± 30	463 ± 18	3.8 ± 0.1
15:58:54–15:59:54	38514	498	-0.8 ± 0.1	272 ± 18	1306 ± 27	3.2 ± 0.1
15:59:54–16:00:54	42027	518	-0.8 ± 0.1	244 ± 15	1319 ± 26	3.5 ± 0.1
16:00:54–16:01:53	26937	328	-0.9 ± 0.1	251 ± 20	807 ± 19	3.5 ± 0.1
16:01:53–16:02:53	14323	256	-0.6 ± 0.1	194 ± 18	477 ± 14	3.6 ± 0.1
16:02:53–16:04:52	3896	267	-0.7 ± 0.1	202 ± 18	286 ± 8	3.7 ± 0.1
16:04:52–16:06:51	3225	212	-0.7 ± 0.1	194 ± 19	194 ± 6	3.9 ± 0.1
16:06:51–16:08:50	3435	269	-0.3 ± 0.2	136 ± 13	197 ± 6	4.1 ± 0.1
16:08:50–16:10:49	2864	241	-0.4 ± 0.2	147 ± 14	169 ± 5	4.1 ± 0.1
16:10:49–16:12:48	3368	310	-0.1 ± 0.2	121 ± 10	189 ± 5	4.2 ± 0.1
16:12:48–16:14:47	3136	231	-0.6 ± 0.2	156 ± 15	191 ± 6	4.2 ± 0.1
16:14:47–16:16:46	3386	283	-0.4 ± 0.2	142 ± 13	210 ± 6	4.1 ± 0.1
16:16:46–16:18:45	3091	283	-0.3 ± 0.2	135 ± 12	215 ± 6	4.1 ± 0.1
16:18:45–16:20:44	2684	198	-0.7 ± 0.2	176 ± 19	226 ± 7	4.1 ± 0.1
16:20:44–16:22:43	2223	217	-0.2 ± 0.2	136 ± 14	231 ± 8	4.1 ± 0.1
16:22:43–16:24:42	1754	153	-0.5 ± 0.2	158 ± 19	232 ± 9	4.0 ± 0.1
16:24:42–16:26:41	1254	94	-0.7 ± 0.2	185 ± 28	266 ± 13	4.0 ± 0.2
16:26:41–16:28:40	871	58	-0.8 ± 0.3	197 ± 37	338 ± 21	4.0 ± 0.2
17:33:40–17:58:16	6107	469	-0.7 ± 0.1	249 ± 17	73 ± 2	3.3 ± 0.1
19:03:16–19:39:22	17051	1810	-0.0 ± 0.1	140 ± 5	88 ± 1	3.7 ± 0.1
20:44:22–21:08:29	2309	277	0.1 ± 0.2	117 ± 11	35 ± 1	4.2 ± 0.1
22:13:29–22:49:35	2603	313	0.3 ± 0.2	91 ± 8	15.6 ± 0.6	4.7 ± 0.2
23:54:47–00:18:47	311	68	2.0 ± 0.9	55 ± 11	5.6 ± 0.6	4.9 ± 0.4
01:23:51–02:00:21[e]	283	55	1.7 ± 0.8	48 ± 10	2.5 ± 0.2	6.0 ± 0.5
03:05:44–03:29:14[e]	59	12	-2.6 ± 0.2	⋯	1.1 ± 0.3	⋯
04:34:04–05:11:04[e]	39	6	-2.7 ± 0.2	⋯	0.5 ± 0.1	⋯

Notes.
[a] $\Delta TS = TS_{PLEXP} - TS_{PL}$
[b] Photon index from best-fit model. The PL is defined as $\frac{dN(E)}{dE} = N_0 E^{\Gamma}$ and the PLEXP as $\frac{dN(E)}{dE} = N_0 E^{\Gamma} \exp\left(-\frac{E}{E_c}\right)$ where E_c is the cutoff energy.
[c] From the fit with the PLEXP model.
[d] Integrated flux between 100 MeV and 10 GeV calculated for the best-fit model.
[e] These intervals are during 2017 September 11.

the significance of the detection. Here we define TS as twice the increment of the logarithm of the likelihood obtained by fitting the data with the source and background model component simultaneously. The TS of the PL fit (TS_{PL}) indicates the significance of the source detection under the assumption of a PL spectral shape, and the $\Delta TS = TS_{PLEXP} - TS_{PL}$ quantifies how much more a complex spectral hypothesis improves the fit. Note that, according to Wilks' theorem (Wilks 1938), the significance of a source (σ) can be roughly approximated as $\sqrt{TS_{PL}}$, and the improvement (in σ) obtained by adding an exponential cutoff to the model can be approximated as $\sqrt{\Delta TS}$.

In Table 1 we list the TS_{PL}, ΔTS, Γ, the photon index for the best-fit model (PL when $\Delta TS < 25$ or PLEXP when $\Delta TS \geqslant 25$)[9] and PLEXP cutoff energy. For several intervals $\Delta TS > 25$, indicating that PLEXP provides a significantly better fit than PL. For these intervals we fit a series of pion-decay models to the data to determine the best proton spectral index following the same procedure described in Ajello et al. (2014). Note that the TS values for PLEXP and pion-decay fits cannot be directly compared (Wilks 1938) because they are not nested models. However, the PLEXP approximates the shape of the pion-decay spectrum; thus we expect the pion-decay models to provide a similarly acceptable fit.

From both Table 1 and Figures 1 and 2 we see that the proton index steepens during the impulsive phase of the flare (from 15:58–16:08 UT) plateaus (or even hardens) from roughly 16:08–16:28 UT to a value of 4.0 ± 0.1. During the subsequent orbit, when the Sun comes back into the field of view at 17:33 UT, its value is back to the initial value found during the impulsive phase and proceeds to soften once more. During the prompt emission, the >100 MeV gamma-ray flux traces the prompt HXR flux, and it starts to increase in the second phase (16:08–16:28 UT). Interestingly, the values of the photon flux when the Sun is back into the LAT field of view (at 17:33:40 UT) are well below the extrapolated flux from the second phase, requiring that a decrease of the flux happened during *Fermi* night-time. The flux then increases again, peaking at approximately 19:30, and decreasing after that. There are thus at least three separate peaks in the light curve, implying at least three separate phases in the underlying acceleration agent of the protons.

2.2. Localization of the Emission

This flare is bright enough to do a time-resolved localization study. Similar to the situation of the 2012 March 7 flares

[9] The value $\Delta TS = 25$ roughly corresponds to 5σ, or a p-value of 3×10^{-7}.

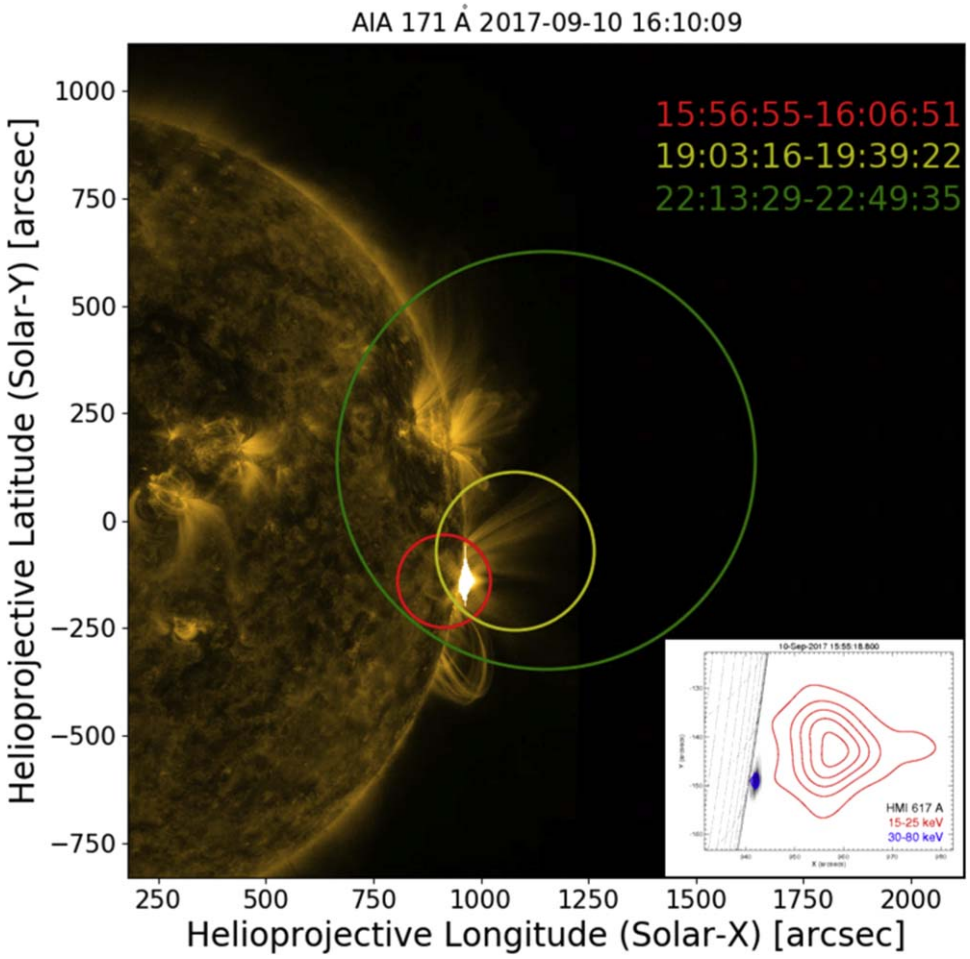

Figure 3. Localization evolution for three different time intervals, overlaid on the *SDO*/AIA 171 image of the Sun at 16:10:09 UT. The circles are the 95% c.l. localization error (plus systematics) for the three different time windows of Table 2 (red: 15:57–16:07; yellow: 19:03–19:39; and green: 22:13–22:50). On the lower-right corner: *RHESSI* contours in the thermal (red) and non-thermal (blue) range are shown on a HMI difference image (the dark is enhanced emission). The scale of the insert is such that both the thermal and non-thermal emissions are contained in the LAT 95% error circle.

Table 2
Evolution of the *Fermi*-LAT Gamma-Ray Source Localization with Fisheye Correction for the 2017 September 10 Flare

Date and Time 2017-09-10 (UT)	HelioX (arcsec)	HelioY (arcsec)	Localization Error (95% c.l.) (arcsec)	Distance from AR (arcsec)	Relative Distance
15:56:55–16:06:51	910	−140	90	80	0.8
19:03:16–19:39:22	1090	−70	180	150	0.8
22:13:29–22:49:35	1150	140	490	330	0.7

(Ajello et al. 2014), we face the same difficulties with the fisheye correction: the asymmetric observational profile induces uncertainties that change the apparent position of the gamma-ray source at each time interval, but in a different direction from one orbit to the next (Ackermann et al. 2012). We performed a study of the fisheye effect on the position of the gamma-ray source as a function of the minimum energy threshold used. We find that the uncorrected position changes significantly as the energy threshold is increased, which is what we expect from the fisheye effect: the correction at 60 MeV changes the position by more than two 68% error radii, whereas the correction at 300 MeV, where also the energy dispersion is small ($\Delta E/E < 0.15$) and can be neglected, remains within the 68% error radius. When examining the corrected positions we find that they are somewhat overlapping, with the position of the gamma-ray source above 300 MeV. This could indicate that the systematic error due to the fisheye effect is larger than the 68% statistical error, for this reason we will therefore use the 95% error radius.

In addition, the *Fermi*-LAT localization capabilities are limited by some small systematics errors due to the instrument and the spacecraft alignment. This results in a 10% increase in the localization error, plus an additional 10″ on the error radius (Nolan et al. 2012). These factors are added in quadrature to the 95% error radii shown in Figure 3.

We limit our localization study to the time intervals with longer exposure (>30 minutes) and smaller average off-axis angles (<55°). We select the time windows starting at 15:56 UT, 19:03 UT, and 22:13 UT, and use an energy threshold of 300 MeV. For the first time window we compute the position using the S15 event class immune to pile-up effects and maximize the number of photons collected.

Table 2 gives the corrected positions of the gamma-ray emission for those times[10] and the 95% containment radius (statistical only). In the table we also give the distance between the position of the AR (estimated to HelioX, HelioY = 957, −135 arcsec) and the best position for the gamma-ray source. The last column shows the ratio between this distance and the 95% containment radius. We see that the location of the gamma-ray emission is consistent with the AR for all time windows, which is different than what observed for the 2012 March 7 (Ajello et al. 2014).

3. Discussion

The 2017 September 10 solar flare was an exceptional flare. It was the brightest gamma-ray source in the sky for more than 12 hr and it was associated with the second GLE of this solar cycle (GLE 72). The Sun was in the field of view of the LAT for both the impulsive and extended phase of the solar flare, allowing for very good coverage of the event. The flux behavior of this flare is similar to other long-duration flares; namely, there is a sharp rising and descending peak coincident with the X-ray flaring activity followed by a slow rise and fall in flux over a period of several hours. However, the temporal variation of the estimated proton index does not show a continuous softening with time as was seen for other long-duration flares (such the 2012 March 7 flares; Ajello et al. 2014), but instead there appear to be multiple phases in the evolution of the proton index. Between 15:48 and 16:08 UT, in coincidence with the descending phase of the HXR flare time profile, the proton index softens with values ranging from 3.2 ± 0.1 to 4.0 ± 0.1. During the twenty minutes that followed, both the proton index appeared to harden and when the Sun came back into the field of view of the LAT at 17:33 UT, the proton index had once again hardened to a value of 3.3 ± 0.1 and proceeded to soften for the remaining almost 9 hr of gamma-ray flaring activity. The behavior of the gamma-ray flux, on the other hand, shows a first impulsive episode, followed by increasing flux during 16:07–16:28:40 UT. When the Sun re-entered the LAT field of view, the flux had dropped by a factor of 5, indicating that the flux dropped during *Fermi* night-time. Finally, the flux increased and peaked between 19:03 and 19:39 UTC, smoothly decreasing after that. This behavior seems to suggest multiple (three) proton acceleration phases.

Based on the analysis performed by Mishev et al. (2018), we know that the onset time of GLE 72 as measured by 27 neutron monitors distributed over the globe is at 16:30 UT ± 1 minute (these are proton arrival times at 1 au so that the arrival time is delayed by roughly 3 minutes with respect the gamma-ray photons). In their analysis of GLE 72, Mishev et al. (2018) found that the ratio of Fe/O of the SEPs is low (<0.07 in the 50–100 MeV/n range) consistent with a gradual event and the timing of the GLE 72 is also consistent with a hypothesis of particle acceleration at a coronal shock driven by the CME. Unfortunately, there is a gap in the LAT data from 16:28 to 17:33 UT because the Sun was not in the field of view. However, based simply on the timing of the events, the third peak in the light curve occurs after the GLE onset as well as after the first LASCO C2 appearance of the CME associated with this flare. During this time the X-ray flare had ceased and no other flaring activity was visible. If indeed the protons responsible for the LDGRF emission share the same acceleration mechanism as the SEP population measured at 1 au, then this could also explain the detection of the long-duration high-energy emission component observed in this flare.

Another aspect of this flare is that the location of the gamma-ray emission is consistent with the AR over a time period of more than 6 hr as can be seen in Figure 3, provided that we detected all of the emission; i.e., there was no western movement of the emission pattern to the back side. This behavior is different from what was found for the 2012 March 7 flares (Ajello et al. 2014), where the emission position was inconsistent with a single localization. This is most likely an effect due to the position of the AR on the western limb of the Sun, considering that the LAT can only detect the gamma-rays originating from the protons interacting in the chromosphere on the visible side of the Sun.

The *RHESSI* observations clearly show that the detected non-thermal HXR emissions from the flare ribbons occur above the limb as seen from Earth, without emission from the solar disk (see insert at the bottom right of Figure 3). As gamma-ray producing ions are typically stopped at much lower altitudes than HXR-producing electrons, where the density is much greater, it is expected that gamma-ray photons traveling toward Earth are heavily attenuated or they may even be completely stopped before they escape toward Earth. As also mentioned by Share et al. (2017), for a typical flare loop with accelerated ions having a PL spectrum with spectral index ∼4, the >100 MeV fluence for a source at 88° would be about 15% of that at disk center. This transmission is falling fast, and a precise value depends critically on knowing where the source really is.

It is therefore questionable that the initial impulsive peak seen by LAT is from the flare ribbons. However, the currently available data is inconclusive regarding the nature of the initial impulsive component.

A more detailed analysis of the gamma-ray flare together with the GLE and CME properties is necessary in order to better understand the connection between the accelerating agents of the proton populations responsible for the emission detected by the LAT and the SEP measured at Earth. In the past years, gamma-ray emission (<100 MeV) has been detected together with GLE in two events (Cliver et al. 1993; Debrunner et al. 1997; Chupp & Ryan 2009), but this is the first time that long-duration GeV gamma-ray emission has been detected together with a GLE. This serves as a precious case study for the acceleration mechanisms at work.

The *Fermi*-LAT Collaboration acknowledges support for LAT development, operation and data analysis from NASA and DOE (United States), CEA/Irfu and IN2P3/CNRS (France), ASI and INFN (Italy), MEXT, KEK, and JAXA (Japan), and the K.A. Wallenberg Foundation, the Swedish Research Council and the National Space Board (Sweden). Science analysis support in the operations phase from INAF (Italy) and CNES (France) is also gratefully acknowledged. This work performed in part under DOE Contract DE-AC02-76SF00515.

ORCID iDs

Nicola Omodei https://orcid.org/0000-0002-5448-7577
Melissa Pesce-Rollins https://orcid.org/0000-0003-1790-8018
Francesco Longo https://orcid.org/0000-0003-2501-2270

[10] We list the mean time of the interval in the table and in Figure 3.

References

Ackermann, M., Ajello, M., Albert, A., et al. 2012, ApJS, 203, 4
Ackermann, M., Ajello, M., Albert, A., et al. 2014, ApJ, 787, 15
Ackermann, M., Allafort, A., Baldini, L., et al. 2017, ApJ, 835, 219
Ajello, M. A. A., Allafort, A., Baldini, L., et al. 2014, ApJ, 789, 20
Atwood, W. B., Abdo, A. A., Ackermann, M., et al. 2009, ApJ, 697, 1071
Chupp, E. L., & Ryan, J. M. 2009, RAA, 9, 11
Cliver, E. W., Kahler, S. W., & Vestrand, W. T. 1993, Proc. ICRC (Alberta), 3, 91
Debrunner, H., Lockwood, J. A., Barat, C., et al. 1997, ApJ, 479, 997
Forrest, D. J., Vestrand, W. T., Chupp, E. L., et al. 1985, Proc. ICRC (La Jolla, CA), 4, 146
Kanbach, G., Bertsch, D. L., Fichtel, C. E., et al. 1993, A&AS, 97, 349
Krucker, S., Saint-Hilaire, P., Hudson, H. S., et al. 2015, ApJ, 802, 19
Kuhar, M., Krucker, S., Oliveros, J. C. M., et al. 2016, ApJ, 816, 6
Li, Y., Xue, J. C., Ding, M. D., et al. 2018, ApJL, 853, L15
Longo, F., Omodei, N., & Digel, S. 2017, ATel, 10720, 1
Mattox, J. R., Bertsch, D. L., Chiang, J., et al. 1996, ApJ, 461, 396
Mishev, A., Usoskin, I., Kocharov, L., et al. 2018, Extended European Cosmic Ray Symp. 26/35th Russian Cosmic Ray Conference, Poster #20, https://ecrs18.asu.ru/event/1/contributions/170/contribution.pdf
Murphy, R. J., Dermer, C. D., & Ramaty, R. 1987, ApJS, 63, 721
Nolan, P. L., Abdo, A. A., Ackermann, M., et al. 2012, ApJS, 199, 31
Pesce-Rollins, M., Omodei, N., Petrosian, V., et al. 2015, ApJL, 805, L15
Ryan, J. M. 2000, SSRv, 93, 581
Seaton, D. B., & Darnel, J. M. 2018, ApJL, 852, L9
Share, G. H., Murphy, R. J., Tolbert, A. K., et al. 2017, arXiv:1711.01511
Vestrand, W. T., & Forrest, D. J. 1993, ApJL, 409, L69
Warren, H. P., Brooks, D. H., Ugarte-Urra, I., et al. 2018, ApJ, 854, 122
Wilks, S. S. 1938, Ann. Math. Stat., 9, 60
Winter, L. M., Bernstein, V., Omodei, N., & Pesce-Rollins, M. 2018, ApJ, 864, 39
Yan, X. L., Yang, L. H., Xue, Z. K., et al. 2018, ApJL, 853, L18